Electron Transfer from HiPIP to the Photooxidized Tetraheme Cytochrome Subunit of *Allochromatium vinosum* Reaction Center: New Insights from Site-Directed Mutagenesis and Computational Studies†

Giovanni Venturoli,‡,§ Mahir D. Mamedov,|| Sheref S. Mansy,# Francesco Musiani,⊥ Massimo Strocchi,⊥ Francesco Francia,‡ Alexey Yu. Semenov,|| James A. Cowan,# and Stefano Ciurli*,⊥

Laboratorio di Biochimica e Biofisica, Dipartimento di Biologia, Università di Bologna, Bologna, Italy, Istituto Nazionale per la Fisica della Materia (INFM), UdR di Bologna, Bologna, Italy, A. N. Belozersky Institute of Physico-Chemical Biology, Moscow State University, Moscow, Russia, Department of Chemistry, Ohio State University, Columbus, Ohio, USA, and Department of Agro-Environmental Science and Technology, University of Bologna, Bologna, Italy

Received August 5, 2003; Revised Manuscript Received October 28, 2003

ABSTRACT: The kinetics of electron transfer from reduced high-potential iron−sulfur protein (HiPIP) to the photooxidized tetraheme cytochrome *c* subunit (THC) bound to the photosynthetic reaction center (RC) from the purple sulfur bacterium *Allochromatium vinosum* were studied under controlled redox conditions by flash absorption spectroscopy. At ambient redox potential $E_h = +200$ mV, where only the high-potential (HP) hemes of the THC are reduced, the electron transfer from HiPIP to photooxidized HP heme(s) follows second-order kinetics with rate constant $k = (4.2 \pm 0.2)\ 10^5\ M^{-1}\ s^{-1}$ at low ionic strength. Upon increasing the ionic strength, *k* increases by a maximum factor of ca. 2 at 640 mM KCl. The role of Phe48, which lies on the external surface of HiPIP close to the $[Fe_4S_4]$ cluster and presumably on the electron transfer pathway to cytochrome heme(s), was investigated by site-directed mutagenesis. Substitution of Phe48 with arginine, aspartate, and histidine completely prevents electron donation. Conversely, electron transfer is still observed upon substitution of Phe48 with tyrosine and tryptophan, although the rate is decreased by more than 1 order of magnitude. These results suggest that Phe48 is located on a key protein surface patch essential for efficient electron transfer, and that the presence of an aromatic hydrophobic residue on the putative electron-transfer pathway plays a critical role. This conclusion was supported by protein docking calculations, resulting in a structural model for the HiPIP-THC complex, which involves a docking site close to the LP heme farthest from the bacteriochlorophyll special pair.

The bacterial reaction center (RC)[1] is an integral membrane protein−pigment complex that catalyzes the conversion of light energy into a more stable form of electrochemical energy during the primary processes of photosynthesis. Photooxidation of the bacteriochlorophyll special pair (P) in the RC is followed by a rapid reduction of $P^{+\bullet}$. In the case of RCs constituted by the three subunits L, M, and H, as structurally determined in *Rhodobacter sphaeroides*, the direct electron donor to $P^{+\bullet}$ is a water-soluble cytochrome c_2 (*1*). In RCs containing an additional membrane-associated c-type tetraheme cytochrome subunit (THC), structurally characterized in *Blastochloris* (*Blc*., formerly, *Rhodopseudomonas*) *viridis* (*2*, *3*), the THC protrudes away from the RC into the periplasm. In *Blc. viridis*, the four heme groups are arranged in the linear sequence P/c-559/c-552/c-556/c-554 with alternating reduction potential values of +380, +20, +310, and −60 mV, respectively (*4*, *5*). This arrangement is conserved in all THCs (*6* and references therein). In *Blc. viridis*, when the two high-potential hemes (c-559 and c-556) are reduced prior to light excitation, it is found that c-559 directly reduces the photooxidized $P^{+\bullet}$ and is itself subsequently reduced by c-556 (*7*, *8*). In a following step, the photooxidized THC is reduced by cytochrome c_2, cytochrome c_8, or high-potential iron−sulfur protein (HiPIP), depending on the bacterial species (*9*).

† This research was supported by NATO Linkage (Grant LST. CLG.978568) and INTAS (Grant 01-483) (to S.C. and A.Y.S.), by the Russian Foundation for Basic Research (Grant 03.04.48983 to A.Y.S. and Grant 01.04.49268 to M.D.M.), by the International Science and Technology Center (ISTC) (Grant 2296 to A.Y.S.), by the Italian Ministery for University and Research (MIUR, PRIN 2001) and by the Inter-university Consortium for Magnetic Resonance on Paramagnetic Metalloproteins (CIRMMP) to S.C. and F.M., by MIUR (PRIN 2001 and FIRB 2001) to G.V. and F.F., and by the National Science Foundation (NSF Grant CHE-0111161) to J.A.C.

* Corresponding author. Department of Agro-Environmental Science and Technology, University of Bologna, Viale Giuseppe Fanin 40, I-40127 Bologna (Italy). Phone: +39−051−209−6204; FAX: +39−051−209−6203; E-mail: stefano.ciurli@unibo.it.

‡ Laboratorio di Biochimica e Biofisica, Dipartimento di Biologia, Università di Bologna.

§ UdR di Bologna.

|| Moscow State University.

Ohio State University.

⊥ Department of Agro-Environmental Science and Technology, University of Bologna.

[1] Abbreviations: HiPIP, high potential iron sulfur protein; THC, tetraheme cytochrome; RC, reaction center; HP, high potential; LP, low potential; Tris, tris(hydroxymethyl)-aminomethane; LDAO, lauryl dimethylamine *N*-oxide; EPR, electron paramagnetic resonance; NMR, nuclear magnetic resonance; HSQC, heteronuclear single quantum coherence.

10.1021/bi035384v CCC: $27.50
Published on Web 12/20/2003

HiPIPs (*10*) are small (8−10 kDa) redox proteins characterized by reduction potentials in the range of +50 to +450 mV (*11*−*13*) and by a $[Fe_4S_4]^{3+/2+}$ redox couple (*14*). Crystal structures of HiPIPs from *Allochromatium* (*A.*) *vinosum* (formerly *Chromatium vinosum*) (*15*−*18*), *Halorhodospira* (*H.*) *halophila* (*19*), *Rhodocyclus* (*Rh.*) *tenuis* (*20*), *Ectothiorhodospira* (*E.*) *vacuolata* (*21*), *Marichromatium* (*M.*) *purpuratum* (*22*), *Thermochromatium* (*T.*) *tepidum* (*23*, *24*), and *Rhodoferax* (*Rf.*) *fermentans* (*25*) have been determined. HiPIPs are abundant in most species of purple phototrophic bacteria that lack cytochrome c_2 and feature a RC-bound THC subunit (*26*). Despite early spectroscopic studies indicating photoinduced formation of oxidized HiPIP by *A. vinosum* chromatophores (*27*, *28*), only in recent years has the involvement of HiPIPs in the photosynthetic machinery of phototrophic bacteria been firmly established. Studies performed on membranes isolated from *Rf. fermentans* (*29*, *30*) and on whole cells of *Rubrivivax* (*Ru.*) *gelatinosus* (*31*) provided the first direct evidence for a physiological role of HiPIP as the reductant of photooxidized THC. A detailed investigation of the kinetics of electron transfer between isolated HiPIP and RC from *Rf. fermentans* demonstrated the fast ($t_{1/2}$ = 2.2 μs) rate of reduction of the highest potential heme (c-556) belonging to the RC THC subunit (*32*). Such a high intrinsic value of the electron-transfer rate strongly supports the formation of a complex between HiPIP and the THC, with the electron transfer occurring during the lifetime of this long-lived complex. The involvement of HiPIP as a photoinduced electron-transfer mediator was also reported in studies of whole cells and membrane fragments of phototrophic bacteria such as *Rh. tenuis* (*33*), *E. vacuolata*, *A. vinosum*, *M. purpuratum*, and *Rhodopila* (*R.*) *globiformis* (*34*). Site-directed mutagenesis studies on *Ru. gelatinosus* confirmed these results (*35*, *36*), while a major role of HiPIP in photosynthetic metabolism was also demonstrated through gene knock-out experiments (*37*).

Here we report the results of kinetic studies of the in vitro redox reactivity of *A. vinosum* HiPIP with RC-bound THC, performed under redox-controlled conditions. The role of the highly conserved Phe48, located on the surface of HiPIP within van der Waals contact with the $[Fe_4S_4]$ cluster, was tested using site-directed mutagenesis. The structure of a possible complex between *A. vinosum* HiPIP and THC was calculated using molecular modeling and protein docking procedures.

MATERIALS AND METHODS

Protein Isolation and Purification. A. vinosum cells were grown under anaerobic photosynthetic conditions as previously reported (*38*) except for the use of malate in place of succinate. The isolation of *A. vinosum* solubilized RC was based on a procedure described by Thornber (*39*). Thawed cells of *A. vinosum* were washed twice in 10 mM TrisHCl, pH 8.0 and resuspended in the same buffer. The cells were broken by passing the suspension three times through a precooled French pressure cell at 20 000 psi in the presence of DNAse (50 μg/mL). Unbroken cells and large particles were removed from the membrane suspension by centrifugation at 12 000*g* for 15 min. The chromatophore membranes were pelleted at 110000*g* for 2 h at 4 °C in a Beckman 50.2 Ti rotor. A stock solution of lauryl dimethylamine-*N*-oxide (LDAO, 30%) was added dropwise to a suspension of chromatophore membranes (at an optical density of 50 at 850 nm) to give a final detergent concentration of 0.2%. The resulting suspension was gently stirred in the dark for 60 min at 25 °C, diluted 10-fold with 10 mM TrisHCl buffer, pH 8.0, and centrifuged for 90 min at 110000*g* at 4 °C. The supernatant was carefully collected and immediately concentrated to 2 mL with an Amicon ultrafiltration cell, fitted with a YM-100 membrane. The sample was then stored at −80 °C.

Reduced wild-type HiPIP was obtained by following the procedure described by Bartsch (*40*). The mutants Phe48Tyr, Phe48Trp, and Phe48Asp were prepared by Quikchange (Stratagene) using 50 ng of pHiPIP template (*41*), 2.5 units of Pfu DNA polymerase (Stratagene), and 125 ng of each primer (Integrated DNA Technologies, Inc). Complementary primers were designed to allow for restriction digest screening via silent mutagenesis. The incorporated restriction site was *Pst*I. For example, the Phe48Tyr pHiPIP primers were 5′-gctgactgccaa***t*****a***c*atgcaggccgacgc***t****gc****a***ggtgctactg-3′ and its exact complement. The bold nucleotides are mutations, the underlined codon is position 48, and the italic region is the engineered *Pst*I site. Identical primers were used for the other mutant constructs except that the appropriate codons were used at codon position 48. The thermocycle was identical to that described in the Quikchange (Stratagene) protocol. An aliquot (20%) of the post-thermocycle sample was then incubated with 5 units of *Dpn*I at 37 °C for 2 h. The mutants Phe48Arg and Phe48His were prepared using the same protocol as previously reported (*70*). Subsequently, $CaCl_2$-competent DH5α cells were transformed via heat shock with the mutant constructs (*42*). After the initial *Pst*I restriction digest screening, all constructs were confirmed by nucleotide sequencing. Mutant HiPIPs were purified as previously described (*41*).

Experimental Measurements. HiPIP concentration was measured at 390 nm using an extinction coefficient of 16 mM^{-1} cm^{-1} (*40*). The kinetics of the electron transfer from reduced HiPIP to the THC in *A. vinosum* RC were studied by flash-spectrophotometry, recording the reduction of photooxidized heme(s) following a single flash at 423 nm under controlled redox conditions. The same kinetics were obtained when the reduction of photooxidized heme(s) was monitored in the α-band region. We chose to analyze quantitatively the results using only the traces obtained in the Soret band due to the much higher (ca. 5-fold) differential extinction coefficient. Absorbance changes, induced by a Xenon flash lamp (3.25 J discharge energy, 4 μs pulse duration at half-maximal intensity) were measured by use of a homemade single beam spectrophotometer, as previously described (*29*). A minimum dark time of 60 s was allowed between repetitive photoexcitation during averaging. The assay mixture contained 50 mM TrisHCl buffer, pH 8.0, and 20 mM KCl. Bacteriochlorophyll concentration in the measuring cuvette was typically 20 μg/mL. By assuming an extinction coefficient $\epsilon_{423} \approx 100$ mM^{-1} cm^{-1}, the concentration of RC photooxidized by a single flash can be estimated as ca. 0.1 μM. The ambient redox potential was measured with a platinum electrode vs. a calomel reference electrode under N_2 flow, as described in ref *43*. Sodium ascorbate (or sodium dithionite for the low potentials) and potassium ferricyanide were used as reductant and oxidant, respectively, in the redox-dependent experimental conditions. Kinetic

measurements were performed in the presence of 10 μM *p*-benzoquinone and 1,2-naphthoquinone as redox mediators. When the solution was redox-poised to reduce the low potential hemes of the THC, 1,4-naphthoquinone, and duroquinone were also added at the same final concentration. All experiments were carried out at 20 °C.

Molecular Modeling and Protein Docking. The sequence of *A. vinosum* THC was aligned with that of *Blc. viridis* and *T. tepidum* using the ClustalW program (*44*), available at http://www.ebi.ac.uk/clustalw, and alignment optimization was carried out using information derived from secondary structure predictions provided by the program JPRED (*45*), available at http://www.compbio.dundee.ac.uk/~www-jpred. The model structure of *A. vinosum* THC was calculated using the program MODELLER 6.2 (*46*) adopting the model-default options, including the hemes in the calculation. The program PROSA II (Version 3.0, 1994) (*47*) was used to test the coherency and validity of the model structure. The Z-scores reported in this work are derived from the standard "hide and seek" procedure of the program, in which the scores are correlated to the difference in potential energy calculated using mean field potentials between the input structure and other randomly assigned folds. Structure validation was performed using PROCHECK (*48*) and WHATIF (*49*). The calculated final structure was deposited in the http://www.postgenomicnmr.net web site. Rigid docking between the calculated model of *A. vinosum* THC and the structure of HiPIP, available in the Protein Data Bank with the code 1CKU (*18*), was performed using the program AUTODOCK 3.0 (*50*). HiPIP was initially placed in a cubic box centered 30 Å away from the Fe atom of LP_2. The THC molecule was used to generate spatial potential energy grids of 124 × 124 × 124 points spaced by 0.35 Å within this box taking into account steric, electrostatic, and hydrogen bonding interactions. Electrostatic solvent screening was modeled using a distance dependent dielectric function (*51*). Hydrogen atoms on THC and HiPIP were added using the program PROTONATE in the AMBER6 program package (*52*). The atomic charges for protein atoms were taken from the AMBER6 force field. The charges for the oxidized heme groups were defined as previously described (*53*), while charges for the reduced $[Fe_4S_4(SCys)_4]^{2-}$ core of HiPIP were taken from ref *54*. HiPIP was placed at random positions within the grid and the possible complexes with low interaction energy were searched using Monte Carlo simulated annealing and roto-translational steps of 30° and 1 Å, respectively. A total of 500 models were generated. Each model was obtained by 100 Monte Carlo cycles at progressively lower temperatures using the default program parameters. This local search is analogous to energy minimization, and finds a local minimum. The final models were clustered on the basis of the distance between LP_2 on the THC and Phe48 on HiPIP, and the best model was chosen on the basis of energy criteria. The protein−protein interface of the docked complex was analyzed by the Protein−Protein Interaction server (http://www.biochem.ucl.ac.uk/bsm/PP/server) (*55*, *56*).

RESULTS

Even though the structure of the *A. vinosum* THC is not known, the extensive sequence homology of the THC subunits over several bacterial species suggests similar molecular structures and, in particular, the presence of four c-type heme groups (*6* and references therein). In *A. vinosum*, the four hemes are distributed along the THC subunit in the sequence P/c-555/c-553/c-555/c-553, and are characterized by reduction potentials of +360 ± 30, +10, +330 ± 30, and +10 mV, respectively (*57* and references therein). Henceforth, the corresponding hemes will be denoted as HP_1, LP_1, HP_2, and LP_2, where HP represents high potential and LP indicates low potential.

The following experiments were carried out to verify the integral functionality of *A. vinosum* solubilized RC obtained by our protocol. The amplitude of the absorbance change induced by a single flash experiment on *A. vinosum* RC is shown in Figure 1A as a function of wavelength. Spectra were obtained at a defined redox potential (E_h) of +200 mV (filled circles) and −50 mV (open circles). Under the first redox condition only the two HP hemes are reduced in the THC before the flash, while at the lower potential all four hemes are reduced. The spectrum obtained at −50 mV shows a small but significant red shift and a slight decrease in amplitude with respect to that measured at +200 mV, indicating that at these two different redox potentials, different hemes are oxidized by the flash. This small shift of the Soret band in the photoinduced difference spectrum taken at high and low redox potentials is consistent with the previously reported small differences in the Soret (*58*) and α-bands (*59*) of the HP and LP hemes. A redox titration of the absorbance changes induced by two flashes fired 200 ms apart at the maximum difference spectrum in the Soret region (423 nm), between 200 and 450 mV, yielded data that were fitted using two Nernstian components, as suggested by EPR spectroscopy (*57* and references therein). This fit provided values of +364 ± 32 and +345 ± 38 mV for HP_1 and HP_2, respectively (not shown). These collective evidences prompted us to use the isolated *A. vinosum* RC for subsequent studies of the kinetics of light-induced electron transfer with reduced HiPIP.

Figure 1B shows the changes in absorption induced at 423 nm by a single flash excitation of *A. vinosum* RC poised at E_h = +200 mV. At this redox potential, in the absence of any added soluble protein electron donor, a single flash induced a rapid decrease of absorbance, corresponding to HP heme(s) oxidation (trace a), with no further changes being detected for up to 90 ms. Upon addition of 20 μM native HiPIP, reduction of the photooxidized HP heme(s) occurred, resulting in the decay of the flash-induced signal (trace b). Faster decay kinetics was observed when the HiPIP concentration was increased to 90 μM (trace c). Over this range of HiPIP concentrations, as shown by the continuous curves in Figure 1B, the reduction kinetics of HP heme(s) were accurately fit to a single-exponential decay, suggesting a pseudo-first-order of reaction. This is confirmed by the linear dependence of the rate constant on HiPIP concentration (Figure 1C). From the slope of the straight-line fitting of the data in Figure 1C, a true second-order rate constant of (4.23 ± 0.18) 10^5 M^{-1} s^{-1} was estimated.

Even at the highest HiPIP concentration used (see Figure 1B, trace c) no decrease in the extent of HP heme(s) photooxidation was observed, indicating that no fast phase reduction occurred within the time resolution of our experimental conditions. These observations suggest that electron transfer from HiPIP to the HP heme(s) takes place in a

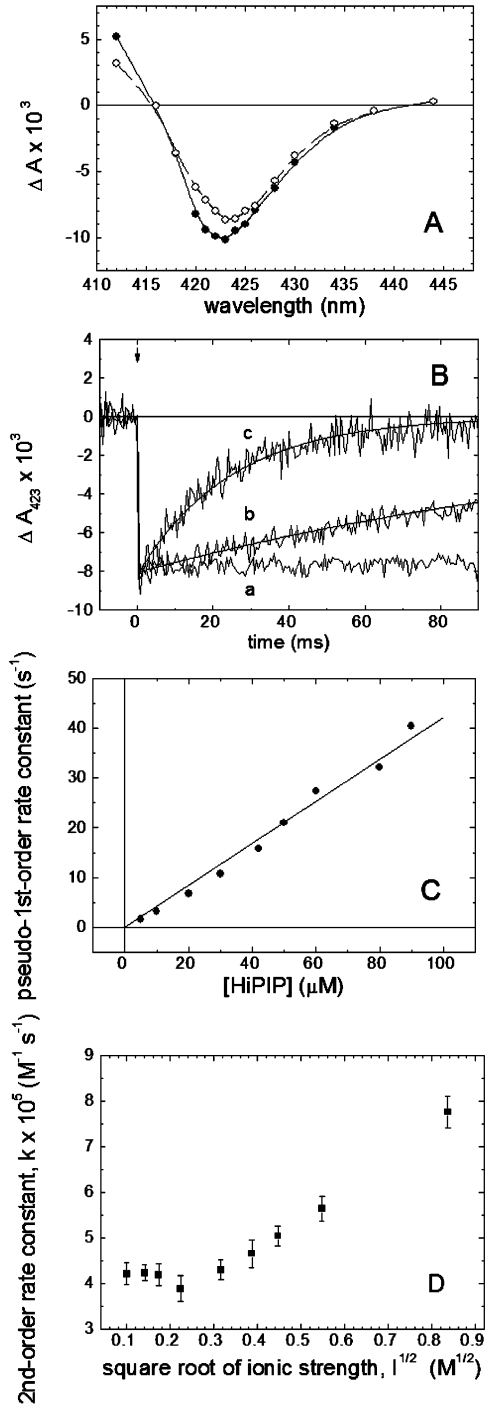

FIGURE 1: (A) Spectrum of absorbance changes induced by a single flash in *A. vinosum* RC poised at a redox potential $E_h = +200$ mV (closed circles) and $E_h = -50$ mV (open circles). (B) Kinetic traces of flash-induced absorbance changes at 423 nm in the absence (trace a) and in the presence of 20 and 90 μM HiPIP (traces b and c, respectively). Assay conditions are described under Materials and Methods. Kinetic traces are the average of four measurements, and the time constant of the instrument was 20 μs. The arrow indicates the time of the light flash. Continuous lines are best fits to exponential decays characterized by rate constants of 6.7 s^{-1} (curve b) and 40 s^{-1} (curve c). (C) Dependence of the observed rate constant upon HiPIP concentration. Values of the pseudo-first-order rate constants were obtained from the decay of flash-induced absorbance changes as shown in panel B. The straight line fitting the data corresponds to a second-order rate constant of (4.23 ± 0.18) 10^5 M^{-1} s^{-1}. (D) Ionic strength dependence of the second-order rate constant evaluated from experiments similar to those shown in panel C. Ionic strength was increased by adding NaCl.

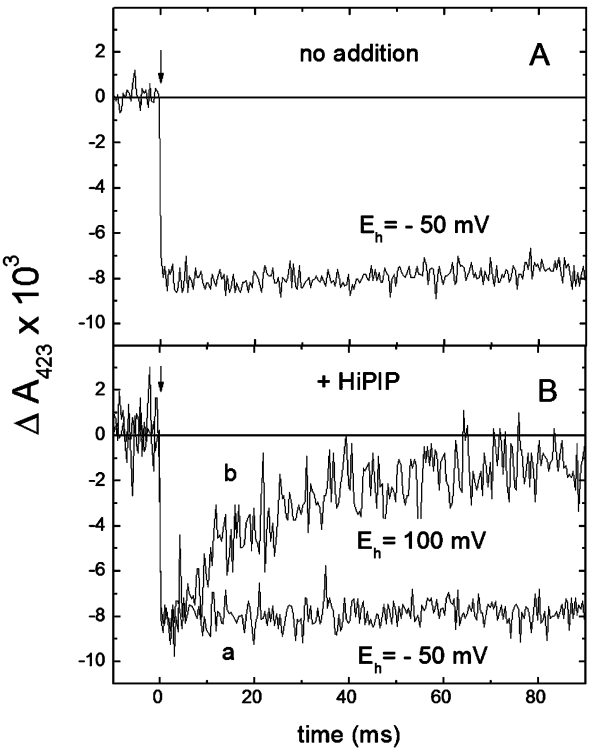

FIGURE 2: Flash-induced absorbance change induced at 423 nm in the absence (A) and in the presence (B) of HiPIP (50 μM) at two different redox potentials, $E_h = -50$ mV (curve a) and $E_h = +100$ mV (curve b). Assay conditions are described under Materials and Methods. The trace in panel A is the average of two measurements, while traces a and b, in panel B, are the result of four averages and of a single measurement, respectively. The instrument time constant was 20 μs.

collisional reaction involving the free soluble protein, and that no functional long-lived complex is formed between HiPIP and the THC. The second-order rate constant for this reaction did not depend on ionic strength, within experimental error, in the range 0.1−0.3 $M^{1/2}$ (Figure 1D). At higher values of ionic strength, the rate constant increased monotonically, with a maximum factor of 2 at about 0.8 $M^{1/2}$. These small changes suggest that the collisional reaction between the redox partners is predominantly governed by hydrophobic forces.

On the basis of the midpoint potentials of HiPIP, HP, and LP hemes, it is expected that reduced HiPIP can only equilibrate with the photooxidized HP hemes. This was confirmed, in our case, by the data shown in Figure 2. Figure 2A shows the flash-induced absorption changes at 423 nm at $E_h = -50$ mV, when all four hemes are reduced before the flash, in the absence of donor protein. Addition of HiPIP (Figure 2B, curve a) did not affect either the amplitude or the kinetics of the absorption changes. Only when the potential was raised back to $E_h = +100$ mV (when both LP hemes are oxidized and only the HP hemes are reduced) was a complete reduction observed in the presence of HiPIP. The inability of HiPIP to reduce the bound THC when all four hemes are reduced reflects an equilibrium distribution for the electron among all redox centers, including $P^{+\bullet}$, HP, and LP hemes as well as HiPIP (thermodynamic control as opposed to kinetic control of the reaction).

To elucidate the details of the redox interaction between the HiPIP and the HP hemes, we examined the effect of point

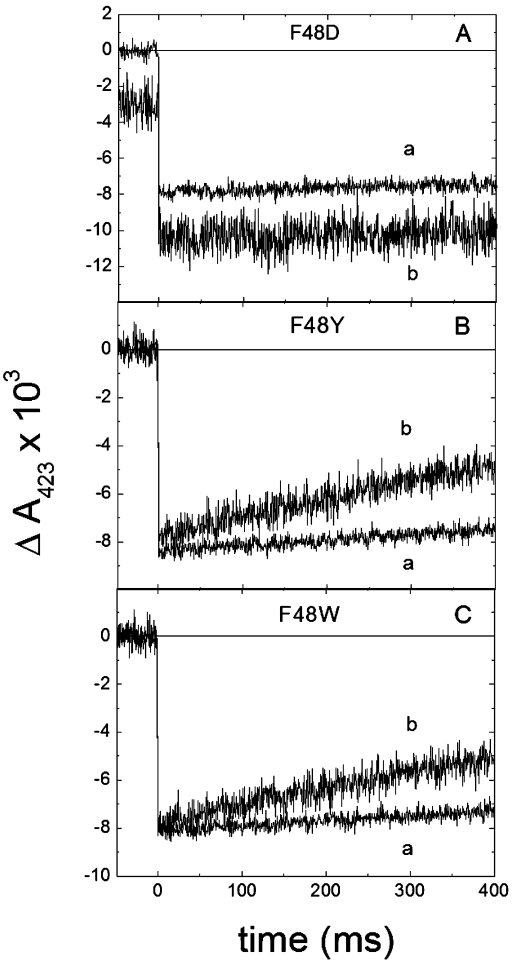

FIGURE 3: Reduction kinetics of photooxidized HP heme(s) by HiPIP mutants Phe48Asp (A), Phe48Tyr (B), and Phe48Trp (C). Traces a and b were recorded in the absence and in the presence of HiPIP, respectively. Added HiPIP concentrations were 106, 90, and 83 μM for Phe48Asp, Phe48Tyr, and Phe48Trp mutants, respectively. Assay conditions are described under Materials and Methods. The ambient redox potential was poised at +200 mV. Traces in the absence of HiPIP (a) are the average of four measurements, while those in the presence of HiPIP (b) are the average of eight measurements.

mutations of Phe48, a highly conserved residue lying on the external surface of HiPIP, protecting the $[Fe_4S_4]$ cluster from solvent. The kinetics of electron donation from HiPIP mutants Phe48Arg, Phe48Asp, Phe48His, Phe48Tyr, and Phe48Trp to HP heme(s) were measured. As shown in Figure 3A, in the presence of Phe48Asp HiPIP, no reduction of the HP heme(s) was observed on the hundreds of millisecond time-scale. The same behavior was observed with Phe48Arg and Phe48His HiPIPs (data not shown). However, as shown in Figure 3B,C, a detectable reduction of the HP heme(s) was observed upon addition of Phe48Tyr and Phe48Trp HiPIPs. It appears, therefore, that substitution of Phe48 with Asp, Arg, or His completely prevents reduction of HP hemes by HiPIP, whereas substitution of Phe48 with aromatic residues such as Tyr and Trp leads to a markedly decreased, but still detectable, reduction of HP heme(s). This conclusion was confirmed by the concentration dependence of the pseudo-first-order rate constant for heme(s) reduction by the aforementioned HiPIP mutants (Figure 4). From these data, a second-order rate constant of (1.02 $\pm$ 0.08) 10^4 M^{-1} s^{-1} and (0.95 $\pm$ 0.04) 10^4 M^{-1} s^{-1} was estimated for Phe48Tyr and Phe48Trp HiPIPs, respectively. The Phe48Arg, Phe48Asp, and Phe48His HiPIP mutants were unable to reduce HP heme(s) even at high concentration (Figure 4). The second-order rate constant for the aromatic mutants slightly increased with increasing ionic strength, whereas no effect was observed for the Arg, Asp, and His substituted proteins (data not shown).

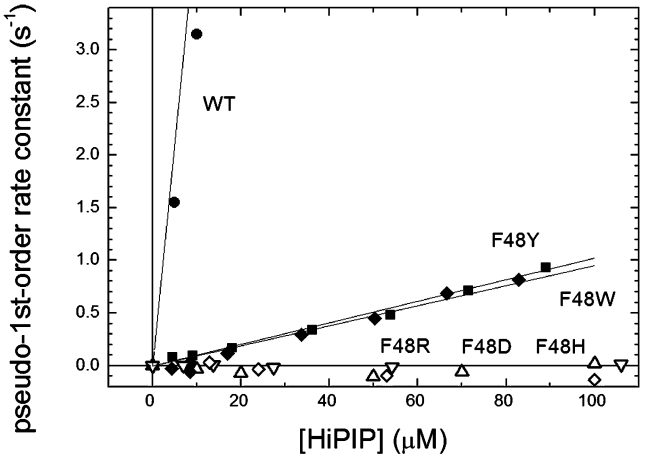

FIGURE 4: Concentration dependence of the pseudo-first-order rate constant for HP heme(s) reduction following a single flash measured in the presence of native (filled circles) and mutated HiPIP: Phe48Tyr (filled squares), Phe48Trp (filled diamonds), Phe48Arg (open triangles), Phe48Asp (open inverted triangles), Phe48His (open diamonds). Pseudo-first-order rate constants were obtained by fitting traces similar to those shown in Figure 3 to an exponential decay. Assay conditions are described under Materials and Methods. The ambient redox potential was poised at +200 mV. Best-fitting straight lines correspond to second-order rate constants of (1.02 $\pm$ 0.08) 10^4 M^{-1} s^{-1} and (0.95 $\pm$ 0.04) 10^4 M^{-1} s^{-1} for the Phe48Tyr and Phe48Trp HiPIPs, respectively. To compare with the rate constant measured in the presence of the native HiPIP, the data of Figure 1C were used, plotting only values at [HiPIP] < 10 μM.

DISCUSSION

We have established the ability of purified HiPIP to reduce photooxidized HP heme(s) in *A. vinosum* RC using kinetic measurements performed in vitro under controlled redox conditions (Figures 1 and 2). The pseudo-first-order character of the reaction kinetics (Figure 1B), the linear dependence of the pseudo-first-order rate constant on HiPIP concentration (Figure 1C), and the absence of any microsecond phase in the kinetics (Figure 1B,C) indicate that the reaction occurs only through a second-order collisional mechanism within a transient complex. The value determined for the second-order rate constant at low ionic strength (4.2×10^5 M^{-1} s^{-1}) doubles at 640 mM KCl (Figure 1D). This value should be compared with the only other available data in the literature for in vitro systems, reporting $k = 4.8 \times 10^7$ and $k = 5.4 \times 10^6$ for the same constant at low and high ionic strength in *Rf. fermentans* purified HiPIP and RC (*32*). Other data for the HiPIP−THC interaction have been reported for in vivo systems (*31*, *33*, *34*), and the actual values for the second-order rate constant cannot be estimated due to the lack of knowledge on the effective HiPIP concentration in the periplasmic space. It is evident that in *A. vinosum* the measured value for k is from 1 to 2 orders of magnitude smaller than that for *Rf. fermentans*, and that the solution conditions are important for dictating the actual value for the second-order process. In particular, the ionic strength has

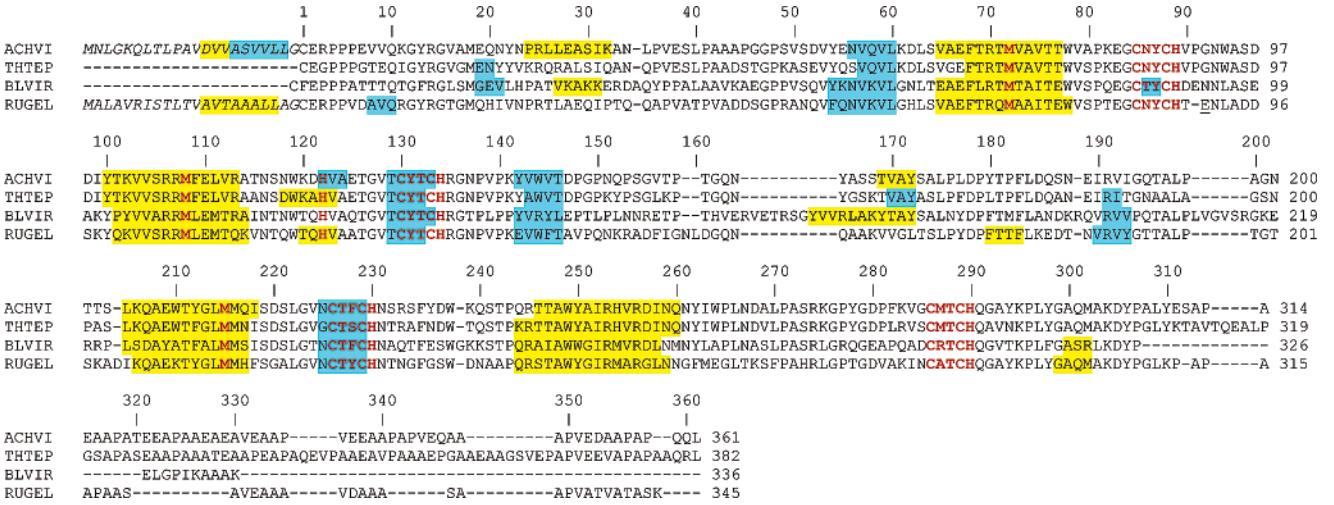

FIGURE 5: Multiple sequence alignment of THC from *A. vinosum* (ACHVI) with THC from *T. tepidum* (THTEP), *Blc. viridis* (BLVIR), and *Ru. gelatinosus* (RUGEL), as obtained from ClustalW and optimized using JPRED. The predicted secondary structure elements are highlighted in yellow (helices) and turquoise (sheets). The residues involved in the heme binding sites are shown in red bold. The residues in italics were not modeled because of the absence of structural data for the homologous proteins. The sequences of *A. vinosum* and *Ru. gelatinosus* were taken from the National Center for Biotechnology Information database, under the accession codes AAA23314 and AAB41578, respectively, while the sequences of *T. tepidum* and *Blc. viridis* were taken from the PDB codes 1EYS and 1DXR, respectively.

different effects depending on the nature of the electrostatic interaction between the two partner proteins: while in the *Rf. fermentans* system the HiPIP−THC interaction involves opposite charges, in *A. vinosum* the interaction between HiPIP and the THC is predominantly hydrophobic.

Due to the similarity of the optical spectra of the two HP hemes, it is impossible to distinguish which of the two hemes is involved in this reaction using time-resolved optical spectroscopy. The time constants for the reaction between soluble electron carriers and the THC subunit (range of milli- to microseconds) are in many species at least 1 order of magnitude larger than the time constants for the interheme electron transfer within the THC subunit (range of micro- to nanoseconds) (*8*, *60*−*62*). Our data show that the same situation holds for the interaction between HiPIP and THC in *A. vinosum*. This generally implies that regardless of which heme reacts with the soluble electron donor, the electron hole generated by P photooxidation will rapidly distribute among the THC hemes before equilibrating with soluble carriers. In the case of *Blc. viridis* it was shown that when both HP hemes are initially reduced, HP_1 (cyt c-559) is oxidized by $P^{+\bullet}$ and subsequently reduced by HP_2 (cyt c-556) in the microsecond time range (*7*, *8*). In *A. vinosum*, since HP_1 and HP_2 are nearly equipotential, the photogenerated electron hole is likely to equilibrate between the two hemes.

The inability of reduced HiPIP to equilibrate with the LP hemes (Figure 2) is consistent with previous results on *Ru. gelatinosus* whole cells (*31*) and membrane fragments (*63*). The reduction of HP hemes by HiPIP can in principle proceed through direct electron donation, or else through an "uphill" step, involving transient reduction of the LP heme(s) followed by a thermodynamically favorable intramolecular electron transfer to the HP heme(s) (*64*). The latter possibility is supported by photoinduced redox kinetics involving *Ru. gelatinosus* THC mutants and HiPIP (*35*, *36*). In fact, Osyczka et al. suggested that the HiPIP−THC binding site is located in the vicinity of the lowest-potential heme, LP_2, and that the electron transfer proceeds uphill from HiPIP to LP_2. This interpretation prompted the same conclusion in a report describing the crystal structure of RC and HiPIP from *T. tepidum* (*23*). The "uphill" model is also supported by kinetic data on the electron donation from soluble c-type cytochromes to the THC subunits in *Blc. viridis* (*62*, *65*) and *Ru. gelatinosus* (*36*, *66*).

The role of the residues located on the most conserved surface patch of HiPIP (*67*) has not been investigated so far in terms of electron transfer reactions with the RC-bound THC. One of these residues, Phe48, is spatially close to the $[Fe_4S_4]$ cluster, and has previously been suggested to mediate electron transfer between the inorganic cluster and the redox partners of HiPIP on the basis of electron self-exchange rate constant measurements (*68*−*70*). Here, the kinetics of photoinduced electron transfer involving HiPIPs with Phe48 replaced by Asp, Arg, His, Tyr, and Trp were investigated. These mutations allowed us to ascertain the effect of substituting this residue with a negative, positive, polar, or aromatic side chain. Substitution of Phe48 with Asp, Arg, or His completely inhibited the reduction of HP heme(s), even when the HiPIP mutant was present in large excess over the RC. Interestingly, when Phe48 was replaced by Tyr or Trp, the HiPIP mutants were still able to donate electrons to the HP heme(s), although at a strongly reduced rate. The dramatic effects observed upon replacement of Phe48 cannot be attributed to any significant structural changes in the mutants, as evaluated by ^1H-^{15}N HSQC NMR spectroscopy experiments (*71*, *72*). Moreover, the mutant proteins showed no optical spectral changes with respect to wild type (data not shown). Therefore, the observed effects on the electron-transfer rate cannot be attributed to major structural alterations due to the point mutations.

The measured reduction potential of the HiPIP mutants used in this work differ, at most, by only ca. 25 mV from that of the wild-type protein ($E^{\circ\prime} = +345$ mV (*70*)).[2] The effects of these changes on the rate constant can be evaluated

[2] The reduction potential for F48H and F48R were previously determined (*70*, *71*), while for F48Y, F48W, and F48D the potential was measured using direct electrochemical methods, obtaining values of +354, +371, and +352 mV.

on the basis of the Marcus equation (*73*) assuming a reorganization energy of 0.8−1.3 eV (*74*, *75*). When either a direct electron transfer to HP_2 (E_m = +330 mV) or an "uphill" mechanism through LP_2 (E_m = +10 mV) is considered, maximal decreases of the rate constants of ca. 40% and ca. 45%, respectively, can be derived as a response to the small reduction potential variations of the mutants. Therefore, the observed decrease of the rate constant in the HiPIP Phe48 mutants cannot be accounted for by a variation of the free energy of electron transfer for none of the HiPIP mutants.

The results described here indicate that Phe48 is crucial in the overall process of electron transfer from HiPIP to the RC-bound THC. In principle, the role of this residue could be to optimize the HiPIP−THC interaction surface and/or to modulate the electron-transfer pathway from the $[Fe_4S_4]$ cluster to the HP heme(s) in the transient collisional complex. Our data cannot distinguish between these two possibilities. In fact, the total absence of activity upon substitution of Phe48 with a negative, positive, or polar residue would suggest a role in protein recognition, while reduced activity in the presence of a different aromatic residue would suggest a role in the electron-transfer pathway. Further complications arise from the fact that both of these effects could be present simultaneously.

To further characterize this aspect and to explore the viability and structures of protein−protein complexes between HiPIP and THC in *A. vinosum*, a computational approach was attempted. First, a molecular model of the *A. vinosum* THC subunit was obtained through protocols of homology building and structure optimization. A multiple alignment of the sequence of THCs from *A. vinosum*, *Blc. viridis*, *T. tepidum*, and *Ru. gelatinosus* (Figure 5) was used as input for model structure calculations. The final refined structure yielded favorable statistics (PROSA Z-score: −8.69, Ramachandran core = 87.4%, allowed = 11.1%, generously allowed = 1.5%, disallowed = 0%) and was deemed to be a reliable model to use for subsequent steps of automated molecular docking with HiPIP.

The docking procedure was carried out taking into consideration the following experimental points: (i) mutagenesis studies have identified a HiPIP surface patch containing Phe48 as a key player in the formation of the transient complex with THC (this work), and (ii) mutagenesis studies on *Ru. gelatinosus* have identified the region around LP_2 as involved in the electron transfer with HiPIP (*35*, *36*). In the best structural model obtained for the docked complex the HiPIP surface patch close to the $[Fe_4S_4]$ cluster interacts with a flat pocket of the THC subunit (Figure 6A,B). This interaction involves mostly hydrophobic residues, consistent with the observed ionic strength dependence of the electron-transfer rate. The complex possesses a complementary surface area (1253 Å^2), corresponding to 8% of the total THC surface and 34% of the HiPIP surface. The calculated distance between the Fe atom in the LP_2 and the core center of the $[Fe_4S_4]$ cluster is 14.0 Å. Phe48, found to be essential for efficient electron transfer, is located in the region between the LP_2 heme and the $[Fe_4S_4]$ cluster, with the plane of the aromatic ring almost parallel to the plane of the heme group (Figure 6C). Therefore, the calculated structure of the complex suggests that, indeed, Phe48 could be involved both in the modulation of an optimal complex interaction and also in the electron transfer itself.

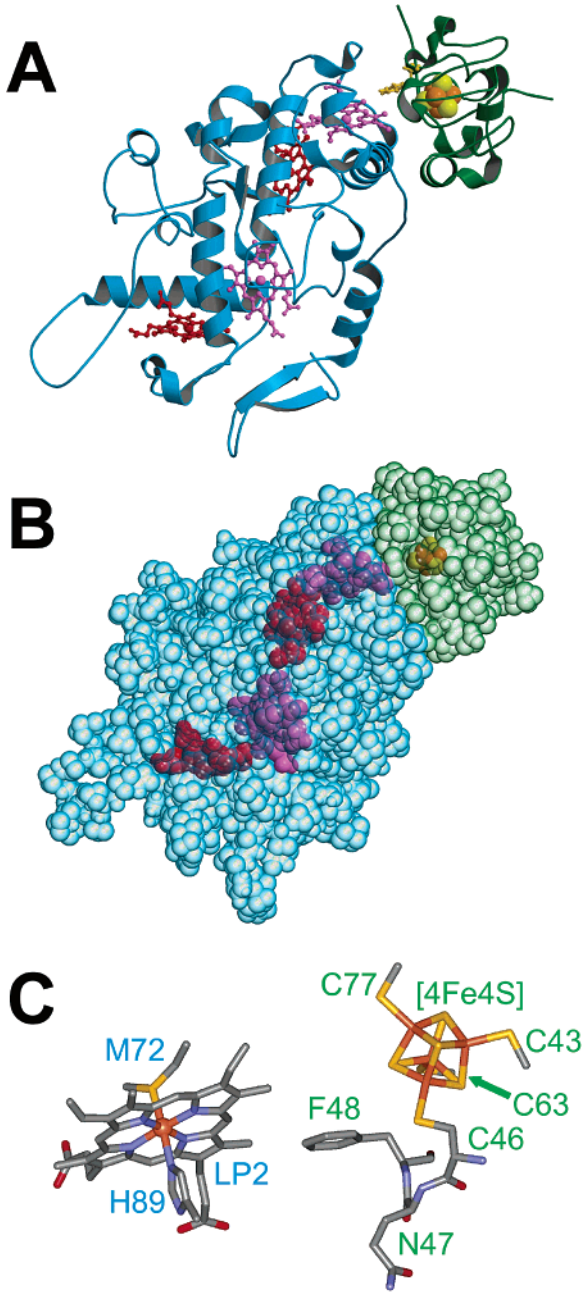

FIGURE 6: (A) Ribbon diagram of the calculated complex between THC (light blue) and HiPIP (dark green). In THC, the HP and LP hemes are represented in red and purple, respectively. In HiPIP, the atoms of the inorganic cluster are represented as yellow (S) and orange (Fe) spheres. The position of Phe48 is highlighted (dark yellow). (B) Space filling diagram of the complex, highlighting the complementary surfaces involved in the interaction as well as the position of the prosthetic groups. (C) A detail of the interaction surface, showing the position of the cluster and Phe48 on HiPIP, and the position of LP_2 and its axial ligands on the THC.

It is important to notice that, in the calculated docked structure, HiPIP interacts with residues Val65, Arg70, and Trp94, corresponding to Val67, Arg72, and Leu96 in *Ru. gelatinosus*. These three residues were found, by site-directed mutagenesis, to be important for the interaction between HiPIP and THC (*35*, *36*). The model of the complex between *A. vinosum* THC and HiPIP was calculated using well-developed protocols of homology building and protein docking. Even though the interaction site is similar to the one proposed for *Ru. gelatinosus* THC and HiPIP (*36*), the

latter derived using manual docking simulations, the relative orientation of the two proteins is significantly different. In particular, the HiPIP molecule is rotated along the axis connecting the $[Fe_4S_4]$ cluster and the LP_2 heme.

In conclusion, this study has provided further insights into the redox reactivity of HiPIPs and THCs in bacterial photosynthesis. Light-induced kinetic measurements coupled to mutagenesis studies on the HiPIP side of the interaction revealed the key role of a surface residue, complementing the information available from site-directed mutagenesis on the THC side.

ACKNOWLEDGMENT

We thank Prof. Marco Borsari for performing the direct electrochemistry experiments on the mutant HiPIPs in his laboratory c/o the Department of Chemistry of the University of Modena (Italy).

REFERENCES

1. Axelrod, H. L., Abresch, E. C., Okamura, M. Y., Yeh, A. P., Rees, D., and Feher, G. (2002) *J. Mol. Biol. 319*, 501−515.
2. Deisenhofer, J., Epp, O., Miki, K., Huber, R., and Michel, H. (1984) *J. Mol. Biol. 180*, 385−398.
3. Deisenhofer, J., and Michel, H. (1989) *Science 245*, 1463−1473.
4. Dracheva, S. M., Drachev, L. A., Konstantinov, A. A., Semenov, A. Y., Skulachev, V. P., Arutjunjan, A. M., Shuvalov, V. A., and Zaberezhnaya, S. M. (1988) *Eur. J. Biochem. 171*, 253−264.
5. Nitschke, W., and Rutherford, A. W. (1989) *Biochemistry 28*, 3161−3168.
6. Nagashima, K. V. P., Sakuragi, Y., Shimada, K., and Matsuura, K. (1998) *Photosynth. Res. 55*, 349−355.
7. Dracheva, S. M., Drachev, L. A., Zaberezhnaya, S. M., Konstantinov, A. A., Semenov, A. Y., and Skulachev, V. P. (1986) *FEBS Lett. 205*, 41−46.
8. Ortega, J. M., and Mathis, P. (1993) *Biochemistry 32*, 1141−1151.
9. Meyer, T. E., and Donohue, T. J. (1995) in *Anoxygenic Photosynthetic Bacteria* (Blankenship, R. E., Madigan, M. T., and Bauer, C. E., Eds.) pp 725−745, Kluwer Academic Publishers, Dordrecht.
10. Carter, C. W., Jr. (2001) in *Handbook of Metalloproteins* (Messerschmidt, A., Huber, R., Wieghardt, K., and Poulos, T., Eds.) pp 602−609, John Wiley, Chichester, UK.
11. Luchinat, C., Capozzi, F., Borsari, M., Battistuzzi, G., and Sola, M. (1994) *Biochem. Biophys. Res. Commun. 203*, 436−442.
12. Banci, L., Bertini, I., Ciurli, S., Luchinat, C., and Pierattelli, R. (1995) *Inorg. Chim. Acta 240*, 251−256.
13. Heering, H. A., Bulsink, Y. B. M., Hagen, W. R., and Meyer, T. E. (1995) *Biochemistry 34*, 14675−14686.
14. Carter, C. W., Jr., Kraut, J., Freer, S. T., Alden, R. A., Sieker, L. C., Adman, E., and Jensen, L. H. (1972) *Proc. Natl. Acad. Sci. U.S.A. 69*, 3526−3529.
15. Carter, C. W., Jr., Kraut, J., Freer, S. T., and Alden, R. A. (1974) *J. Biol. Chem. 249*, 6339−6346.
16. Carter, C. W. J., Kraut, J., Freer, S. T., Xuong, N.-H., Alden, R. A., and Bartsch, R. G. (1974) *J. Biol. Chem. 249*, 4212−4215.
17. Freer, S. T., Alden, R. A., Carter, C. W., Jr., and Kraut, J. (1975) *J. Biol. Chem. 250*, 46−54.
18. Parisini, E., Capozzi, F., Lubini, P., Lamzin, V., Luchinat, C., and Sheldrick, G. M. (1999) *Acta Crystallogr. D55*, 1773−1784.
19. Breiter, D. R., Meyer, T. E., Rayment, I., and Holden, H. M. (1991) *J. Biol. Chem. 266*, 18660−18667.
20. Rayment, I., Wesemberg, G., Meyer, T. E., Cusanovich, M. A., and Holden, H. M. (1992) *J. Mol. Biol. 228*, 672−686.
21. Benning, M. M., Meyer, T. E., Rayment, I., and Holden, H. M. (1994) *Biochemistry 33*, 2476−2483.
22. Kerfeld, C. A., Salmeen, A. E., and Yeates, T. O. (1998) *Biochemistry 37*, 13911−13917.
23. Nogi, T., Fathir, I., Kobayashi, M., Nozawa, T., and Miki, K. (2000) *Proc. Natl. Acad. Sci. U.S.A. 97*, 13561−13566.
24. Liu, L., Nogi, T., Kobayashi, M., Nozawa, T., and Miki, K. (2002) *Acta Crystallogr. D58*, 1085−1091.
25. Gonzalez, A., Benini, S., and Ciurli, S. (2003) *Acta Crystallogr. Sect. D 59*, 1582−1588.
26. Bartsch, R. G. (1991) *Biochim. Biophys. Acta 1058*, 28−30.
27. Kennel, S. J., Bartsch, R. G., and Kamen, M. D. (1972) *Biophys. J. 12*, 882−896.
28. Evans, M. C. W., Lord, A. V., and Reeves, S. G. (1974) *Biochem. J. 138*, 177−183.
29. Hochkoeppler, A., Ciurli, S., Venturoli, G., and Zannoni, D. (1995) *FEBS Lett. 357*, 70−74.
30. Hochkoeppler, A., Kofod, P., Ferro, G., and Ciurli, S. (1995) *Arch. Biochem. Biophys. 322*, 313−318.
31. Schoepp, B., Parot, P., Menin, L., Gaillard, J., Richaud, P., and Vermeglio, A. (1995) *Biochemistry 34*, 11736−11742.
32. Hochkoeppler, A., Ciurli, S., Zannoni, D., Meyer, T. E., Cusanovich, M. A., and Tollin, G. (1996) *Proc. Natl. Acad. Sci. U.S.A. 93*, 6998−7002.
33. Menin, L., Schoepp, B., Parot, P., and Vermeglio, A. (1997) *Biochemistry 36*, 12183−12188.
34. Menin, L., Gaillard, J., Parot, P., Schoepp, B., Nitschke, W., and Vermeglio, A. (1998) *Photosynth. Res. 55*, 343−348.
35. Osyczka, A., Nagashima, K. V. P., Shimada, K., and Matsuura, K. (1999) *Biochemistry 38*, 2861−2865.
36. Osyczka, A., Nagashima, K. V. P., Sogabe, S., Miki, K., Shimada, K., and Matsuura, K. (1999) *Biochemistry 38*, 15779−15790.
37. Nagashima, K. V., Matsuura, K., Shimada, K., and Vermeglio, A. (2002) *Biochemistry 41*, 14028−14032.
38. Thornber, J. P. (1970) *Biochemistry 9*, 2688−2698.
39. Lin, L., and Thornber, J. P. (1975) *Photochem. Photobiol. 22*, 37−40.
40. Bartsch, R. G. (1978) *Methods Enzymol. 53*, 329−340.
41. Agarwal, A., Tan, J., Eren, M., Tevelev, A., Lui, S. M., and Cowan, J. A. (1993) *Biochem. Biophys. Res. Commun. 197*, 1357−1362.
42. Sambrook, J., Fritisch, E. F., and Maniatis, T. (1989) *Molecular Cloning: A Laboratory Manual*, Laboratory Press, Cold Spring Harbor.
43. Venturoli, G., Fernandez-Velasco, J. G., Crofts, A. R., and Melandri, B. A. (1986) *Biochim. Biophys. Acta 851*, 340−352.
44. Thompson, J. D., Higgins, D. G., and Gibson, T. J. (1994) *Nucleic Acid Res. 22*, 4673−4680.
45. Cuff, J. A., Clamp, M. E., Siddiqui, A. S., Finlay, M., and Barton, G. J. (1998) *Bioinformatics 14*, 892−893.
46. Marti-Renom, M. A., Stuart, A. C., Fiser, A., Sanchez, R., Melo, F., and Sali, A. (2000) *Annu. Rev. Biophys. Biomol. Struct. 29*, 291−325.
47. Sippl, M. J. (1993) *Proteins Struct. Funct. Genet. 17*, 355−362.
48. Laskowski, R. A., MacArthur, M. W., Moss, D. S., and Thornton, J. M. (1993) *J. Appl. Crystallogr. 26*, 283−291.
49. Vriend, G. (1990) *J. Mol. Graphics 8*, 52−56.
50. Morris, G. M., Goodsell, D. S., Halliday, R. S., Huey, R., Hart, W. E., Belew, R. K., and Olson, A. J. (1998) *J. Comp. Chem. 19*, 1639−1662.
51. Mehler, E. L., and Solmajer, T. (1991) *Protein Eng. 4*, 903−910.
52. Case, D. A., Pearlman, D. A., Caldwell, J. W., Cheatham, T. E., III, Ross, W. S., Simmerling, C. L., Darden, T. A., Merz, K. M., Stanton, R. V., Cheng, A. L., Vincent, J. J., Crowley, M., Tsui, V., Radmer, R. J., Duan, Y., Pitera, J., Massova, I., Seibel, G. L., Singh, U. C., Weiner, P. K., and Kollman, P. A., 1999, University of California, San Francisco.
53. Banci, L., Bertini, I., Gray, H. B., Luchinat, C., Reddig, T., Rosato, A., and Turano, P. (1997) *Biochemistry 36*, 9867−9877.
54. Banci, L., Bertini, I., Carloni, P., Luchinat, C., and Orioli, P. L. (1992) *J. Am. Chem. Soc. 114*, 10682−10689.
55. Jones, S., and Thornton, J. M. (1995) *Prog. Biophys. Mol. Biol. 63*, 31−65.
56. Jones, S., and Thornton, J. M. (1996) *Proc. Natl. Acad. Sci. U.S.A. 93*, 13−20.
57. Nitschke, W., Jubault-Bregler, M., and Rutherford, A. W. (1993) *Biochemistry 32*, 8871−8879.
58. Parson, W. W. (1969) *Biochim. Biophys. Acta 189*, 397−403.
59. Cusanovich, M. A., and Kamen, M. D. (1968) *Biochim. Biophys. Acta 153*, 376−396.
60. Van Grondelle, R., Duysens, L. N., Van der Wel, J. A., and Van der Wal, H. N. (1977) *Biochim. Biophys. Acta 461*, 188−201.
61. Chen, I.-P., Mathis, P., Koepke, J., and Michel, H. (2000) *Biochemistry 39*, 3592−3602.
62. Ortega, J. M., Drepper, F., and Mathis, P. (1999) *Photosynth. Res. 59*, 147−157.
63. Lieutaud, C., Nitschke, W., Vermeglio, A., Parot, P., and Schoepp-Cothenet, B. (2003) *Biochim. Biophys. Acta 1557*, 83−90.
64. Page, C. C., Moser, C. C., Chen, X., and Dutton, P. L. (1999) *Nature 402*, 47−52.

65. Knaff, D. B., Willie, A., Long, J. E., Kriauciunas, A., Durham, B., and Millett, F. (1991) *Biochemistry 30*, 1303−1310.
66. Osyczka, A., Nagashima, K. V. P., Sogabe, S., Miki, K., Yoshida, M., Shimada, K., and Matsuura, K. (1998) *Biochemistry 37*, 11732−11744.
67. Van Driessche, G., Ciurli, S., Hochkoeppler, A., and Van Beeumen, J. J. (1997) *Eur. J. Biochem. 244*, 371−377.
68. Mizrahi, I. A., Meyer, T. E., and Cusanovich, M. A. (1980) *Biochemistry 19*, 4727−4732.
69. Bertini, I., Gaudemer, A., Luchinat, C., and Piccioli, M. (1993) *Biochemistry 32*, 12887−12893.
70. Soriano, A., Li, D., Bian, S., Agarwal, A., and Cowan, J. A. (1996) *Biochemistry 35*, 12479−12486.
71. Soriano, A., and Cowan, J. A. (1996) *Inorg. Chim. Acta 251*, 285−290.
72. Mansy, S. S., Xiong, Y., Hemann, C., Hille, R., Sundaralingam, M., and Cowan, J. A. (2002) *Biochemistry 41*, 1195−1201.
73. Marcus, R. A. and Sutin, N. (1985) *Biochim. Biophys. Acta 811*, 265−322.
74. Moser, C. C., Keske, J. M., Warmcke, K., Farid, R. S., and Dutton, P. L. (1992) *Nature 355*, 796−802.
75. Venturoli, G., Drepper, F., Williams, J. C., Allen, J. P., Lin, X., and Mathis, P. (1998) *Biophys. J. 74*, 3226−3240.

BI035384V